Extension of The Magic-Angle System in Twisted Bilayer-Graphene by Adjusting Parameter Values

Anirudh Kannan[1] and Chihiro Ikezi[#]

[1]Saint Francis High School, Houston, TX, USA
[#]Advisor

ABSTRACT

Twisted-bilayer graphene (TBG) has attracted significant attention in the world of condensed matter physics in the past few years owing to its unique properties. Consisting of two sheets of graphene, when TBG is rotated by a certain magic angle, it can transition into a remarkable superconducting state. Using the low-energy continuum Hamiltonian model developed by Bistritzer and MacDonald, along with theory on the relationship between tunneling amplitudes and magic angle[1], we change parameters of the model in order to analyze the effect such changes have on the band structure of the overall system. For any twist angle, inputting corresponding amplitude values yields far flatter bands than those yielded by inputting standard amplitude values. Specifically, those models with twist angle and amplitudes lower than those of the conventional model possess flatter bands than the absolute flattest bands hitherto observed.

Introduction

A single graphene sheet consists of hexagonal unit cells of carbon atoms forming a honeycomb lattice, with two interpenetrating triangular sublattices commonly labeled A and B[1,2], as shown in Figure 1A. The momentum-space geometry of graphene consists of a hexagonal reciprocal lattice; at the corners of each hexagonal Brillouin zone are crossings between the valence and conduction bands. These crossings take the shape of a pair of cones, meeting at a single point where the two bands intersect; the cones are known as Dirac cones, and the points as Dirac points[3]. Each Brillouin zone has two sets of three equivalent Dirac points, located at the equivalent K and K' corners of the Brillouin zone[4], as shown in Figure 1B.

TBG is composed of two isolated graphene sheets stacked on top of each other, oriented parallel to each other, and rotated relative to one another by a twist/rotation angle Θ[5]. This stacking configuration results in the formation of a moiré pattern, giving rise to a superlattice[5]. This superlattice is not commensurate; as can be seen in Figure 1C, there are brighter regions of "AA" stacking, where atoms in the two layers are directly above and below each other, as well as darker regions of "AB" or "BA" Bernal stacking, where half of the atoms in the top layer sit above an atom in the bottom layer, and the rest of the atoms in the top and bottom layers sit above the center of a hexagonal unit cell in the bottom and top layers respectively. With regard to momentum space, we see in Figure 1D that each Dirac cone in one layer now has a neighboring Dirac cone in the other layer. Interlayer coupling between the two graphene sheets results in electrons hopping between momentum-space points on both sheets, points on both the same and the opposite sheet. This results in markedly different electronic properties compared to single-layer graphene[6]. Said properties are fundamentally dependent on the extent of coupling between layers, which is itself dependent on the twist angle Θ. For large Θ, the neighboring Dirac cones are widely separated, and the band structure is not heavily influenced by coupling to the opposite layer. When we decrease the twist angle, hybridization and tunneling both increase, and the two layers become more strongly coupled[1].
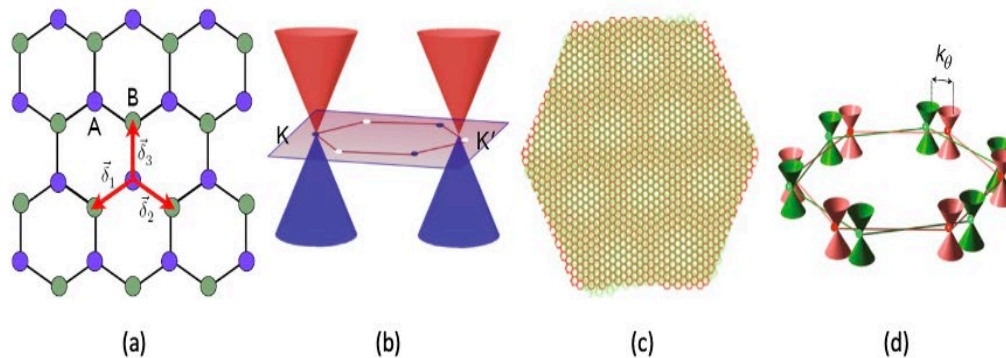
Figure 1. Real and momentum-space structure of single-layer graphene and TBG. (*a*) *A* and *B* sublattices of a single graphene sheet. δ_1, δ_2, and δ_3 are vectors of identical magnitude pointing to the three nearest neighbors (points closest to the chosen point), all of which are on the other sublattice. (*b*) Dirac cones in *k*-space. (*c*) *AA* (light regions) and *AB*/*BA* (dark regions) — the two different sheets are in red and green. (*d*) Dirac cones in top and bottom layers (red and green, respectively). k_Θ is the distance between neighboring cones; its value is dependent on twist angle Θ. Adapted from: (*a*), ref.[7], ISRN; (*b*), (*c*), (*d*), ref.[1], Springer Nature Ltd.

At a series of discrete twist angles, the largest of which is $\Theta \approx 1.05°$, the Fermi velocity at the Dirac points becomes zero, the density of states at the Dirac point increases significantly, and, most notably, the two bands closest to the Dirac point are compressed and become flat bands[8]. The presence of the flat bands is a harbinger of extraordinary electronic properties in the bilayer structure. While the electronic structures of most materials can be effectively explained as a system of non-interacting electrons, those with flat bands are instead considered to be part of a group known as strongly correlated materials[9]. Many strongly correlated materials have strange properties, and TBG is no exception. The system is extremely sensitive to carrier density and band filling and can be extensively tuned with methods such as gating and doping. Extensive manipulation via such techniques has led to the observation of a variety of extraordinary quantum, electrical, and magnetic states in this singular material: TBG has displayed such forms as a correlated insulator, ferromagnet, antiferromagnet, and strange metal, among others[1,10,11]. But by far, the most exciting form it has taken is that of a superconductor; near a correlated insulating phase at half filling, zero resistance has appeared at several of the magic twist angles[12]. The variety and degree of outstanding phenomena observed at these magic angles has served to push TBG to the forefronts of the materials science and condensed matter physics fields.

Demonstrated in a lab setting in 2018, superconductivity in TBG has attracted such high levels of attention because it is believed to potentially be unconventional; that is, it may not conform to any of the postulated theories on the phenomenon[13]. An understanding of superconductivity in TBG would be a massive step towards understanding the phenomenon as a whole. A clearer understanding of superconductivity might well pave the way for the eventual discovery of a room temperature superconductor, which would transform electronics and automation, alleviate energy problems, revolutionize the computing industry, and almost certainly change the world.

Recent studies have shown that it is possible to modulate the degree of interlayer coupling while keeping the twist angle constant; thus, coupling and twist angle can in fact be adjusted independently of one another[4,14]. Furthermore, it is known that the value of the magic angle is in fact linearly proportional to the strength of interlayer coupling[1,9,14,15]. Given this, changing the twist-angle and coupling strength in such a manner that the ratio between them remains the same yields an infinite number of different flat-band systems, each one with its own unique set of parameter values. Herein, we analyze the various band structures of these numerous systems—in particular, the two flat bands themselves. We aim to study the effect that changing the parameter

values has on the flatness and shape of the bands. In doing so, our purpose is to gain a better understanding of how the physical properties of TBG affect its quantum and electronic properties, as well as foresee promising TBG systems that could be examined in a lab setting in the near future.

Methods

The computer model we use is a numerical solution to the TBG model developed by Rafi Bistritzer and Allan MacDonald in 2011, which is valid for all $\Theta < 10°$.

The band structure diagram we use concerns four key points in momentum space: Γ, K_t, K_b, and M. The locations of these points within the reciprocal space moiré Brillouin zone of the lattice are shown in Figure 2.

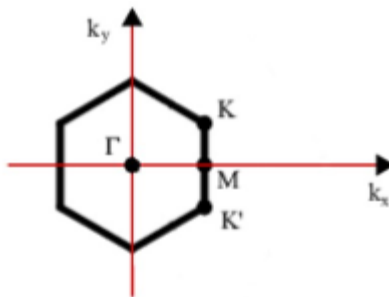**Figure 2.** Momentum-space layout of model. The Γ point is the center of the first Brillouin zone. The K and K' points are the same as K_t and K_b, and represent two inequivalent Dirac cones, one above and one below Γ. M is halfway between the two K points. The latter three points also lie on the edge of the hexagonal Brillouin zone. These four points are utilized because they possess important symmetry in momentum space. Adapted from: ref.[16], IOP.

Interlayer and intralayer hopping amplitudes are quantitative measurements of the frequencies of interlayer and intralayer hopping respectively; equivalently, interlayer hopping is a quantitative measure of the strength of interlayer coupling, and vice versa. As a result of the moiré superlattice being incommensurate, with regions of *AA* patterned and *AB/BA* patterned stacking, we can utilize two different interlayer amplitudes. We denote the interlayer hopping amplitude for AA patterned regions to be w_0, while the interlayer hopping amplitude for *AB/BA* patterned regions is w_1; the intralayer hopping amplitude is denoted t. In TBG, *AB/BA* stacking is more favorable, or more likely to be present at a given location, than *AA* stacking[17]. Thus, $w_1 > w_0$ for traditional TBG systems with reasonable parameter values. In prior studies, the ratio of w_0 / w_1 has been set to a range of values between 0.7 and 0.8[17,18,19,20]; for the purposes of our model, w_0 / w_1 is set to 0.75.

It is known in the literature that the value of the magic twist angle Θ is proportional to the ratio of the interlayer to intralayer hopping amplitudes[1,14,15]. This is due to the peculiar flatness of the bands being a result of the interplay between the momentum-space misalignment of the Dirac cones between the two layers (controlled by twist angle) and the strength of hybridization between layers (controlled by coupling strength)[9]. In a traditional TBG system, the values of the amplitudes are fixed, and thus the magic twist angle is also fixed at 1.05°. Recent studies have suggested that with application of pressure to a traditional system, the strength of interlayer coupling, and by extension the values of w_0 and w_1, can be increased[4]. Alternatively, they can be decreased by either moving the graphene sheets farther apart, or else moving them closer together while intercalating the ions or adding a barrier hBN[14]. Therefore, in a system where the interlaying hopping amplitudes were tuned to be higher, the value of the magic angle would accordingly need to increase for flat bands to be maintained, and vice versa if the amplitudes were decreased. This system, with adjusted parameter values, would nonetheless demonstrate a flat band scheme, or alternatively flatter bands than would be present in the

same material if it possessed any other twist angle value. Simply put, as long as the ratio κ_1 of the twist-angle and the interlayer amplitudes is kept constant, the flat-band (or "flattest-band") scheme ought to be maintained. As the ratio between the two amplitudes w_0 and w_1 is fixed, either one can be used to formulate κ_1. We use w_1; thus, we have that $\kappa_1 = \Theta / w_1$. The specific properties of the system, as well as the exact value of the magic twist angle, are then dependent on the ratio $\kappa_2 = w_1 / t$, or the interlayer-intralayer ratio.

We utilize our model to analyze these "proportional angle-amplitude" systems—those with both higher and lower values of κ_2—by qualitatively examining the effect that increasing and decreasing κ_2 has on the flatness of the flat bands. We also contrast them to "standard-amplitude" systems—those where the w_1 and w_0 values are kept constant even as Θ is changed.

We define the control to be the standard $\Theta \approx 1.05°$ magic-angle model with unaltered amplitude values. It has $\kappa_1 \approx 9.55$, and $\kappa_2 \approx 0.0407$, as shown below:

$$\kappa_1 = \frac{\theta}{w_1} = \frac{1.05}{0.110} \approx 9.55$$

and

$$\kappa_2 = \frac{w_1}{t} = \frac{0.110}{2.7} \approx 0.0407$$

It is the only model that is a member of both the proportional angle-amplitude and standard-amplitude regimes.

We define the flat-band regime to be the set of models for which both bands can be considered "flat". Notwithstanding the colloquial definition of the term, we analytically define it using two metrics: height, referring to the general vertical position of the band or its semi-components relative to y=0, and flatness, referring to the lack of rapid increases or decreases (peaks and valleys, equivalently) in the band structure as we move along the x-axis (through momentum space). For the purpose of analytically measuring the height of the bands, our two metrics are the average height and area (integral) under the bands. We calculate the average height of a band by taking the absolute value of each y-value (energy value) for each momentum-space point along the x-axis, then finding the average of this set. For the purpose of analytically measuring the flatness of the bands, our two metrics are the standard deviation of the average height and the average magnitude of the gradient (the average of the absolute values of the gradient value at every plotted point in momentum space). Any band that is hereby defined to be "flat" must possess both low height and high flatness, as per the definitions above. The control model yields bands that lie close to $y = 0$ and possess neither peaks nor valleys, satisfying these conditions.

Any of Θ, w_1, and w_0 can be chosen for the key dependent variable; we choose w_1, as in a laboratory setting it would be the focus when fabricating the structure itself. To simulate multiple sets of parameter values, we increment or decrement w_1 and then adjust Θ and w_0 accordingly; the value of t is kept constant. For the band structures, our $y = 0$ is set at the energy value corresponding to the intersection of the Dirac cones; thus, all plots will be vertically centered at this energy level. For all graphs, orange represents the top band, blue the bottom.

For the $\Theta > 1.05°$ regime we plot the band structures for $\Theta < 10°$, or $w_1 < 1.05$ eV. We increment w_1 by 5×10^{-3} for each separate model (here, the phrase refers to a series of parameters for which the band structure is plotted). In total, we simulate 188 models for this regime. For the $\Theta < 1.05°$ regime we plot the band structures for $\Theta > 0.18°$, or $w_1 < 0.0189$ eV. We increment w_1 by 1×10^{-3} for each separate model; we simulate a total of 93 models for this regime.

Results

$\Theta > 1.05°$

As shown in Figure 3A, the average height of both the top and bottom bands consistently increases as we increase w_1, and the height of the latter increases more rapidly than that of the former. Furthermore, as shown in Figure 3B, the integral under (over) the bottom band also increases at a very high rate, while the integral under the top band increases at a less prominent rate; the two functions diverge rapidly as we increase w_1. Measurement of both average height and integral yields the result that the difference between the size and height of the top and bottom bands is sizable, clear, and conclusive. Visually, this increase in band size and height as we increase w_1 is also apparent; see the select band structures shown in Figure 3C. While the average heights of the bottom and top bands are initially approximately the same, it is once more visually apparent that the bottom band's average height increases at a far more rapid rate compared to that of the top band. Furthermore, upon reaching $w_1 \approx 0.6$ eV or $\Theta \approx 6°$, the bottom band cannot be considered flat owing to the development of a large, sharp peak at the Γ point, which contrasts with the flatter curve at the same point maintained by the top band.
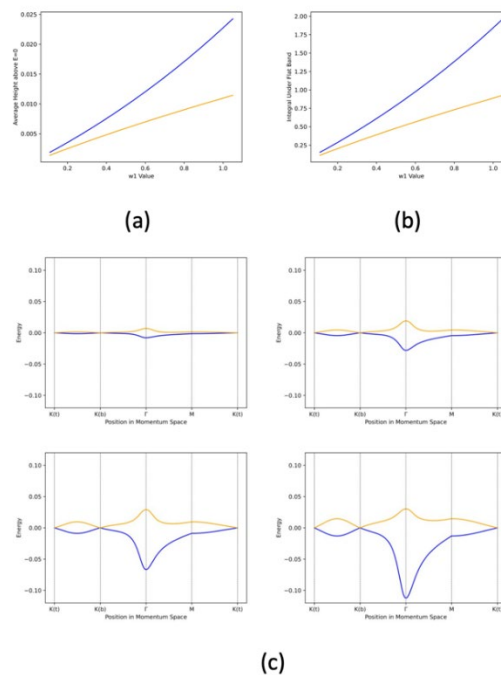

(a)   (b)

(c)

Figure 3. Band height for $\Theta > 1.05°$. (*a*) Average height (energy) of all points making up band. (*b*) Integral under each band (for bottom band, this is instead additive inverse of integral, such that all final values are positive). For (*a*) and (*b*), $y = 0$ is the height of the intersection point of the Dirac cones. Both (*a*) and (*b*) plot both bands for all models in the range of w_1 values for the regime. (*c*) Selected band structures — (*top left*): control model; (*top right*): $w_1 = 0.35\,eV$, or $\Theta \approx 3.34°$; (*bottom left*): $w_1 = 0.71\,eV$, or $\Theta \approx 6.78°$; (*bottom right*): $w_1 = 1.05\,eV$, or $\Theta \approx 10°$.

The standard deviation of height and average magnitude of gradient are displayed in Figures 4A and 4B, respectively. For both, the discrepancy between the bottom and top bands becomes pronounced as we increase w_1. While the top band reaches an asymptote for both these plots, the bottom band increases in both metrics extremely rapidly as we increase w_1. Thus, the top band retains high flatness and variation in height remains low, while the bottom band does not share either of these traits. Visually, this is apparent in the sharp increase and decrease in height about the Γ peak in the bottom band.
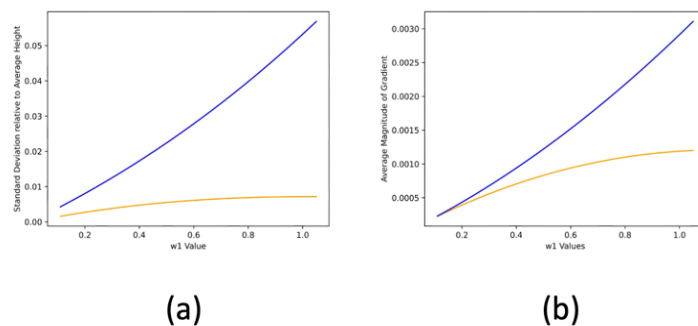
(a) (b)

Figure 4. Band flatness for $\Theta > 1.05°$. (*a*) Standard deviation of heights of all points making up band. (*b*) Average magnitude of gradient (average of absolute values of gradient at each *k*-space point). (*a*) and (*b*) plot both bands for all models in the range of w_1 values for the regime.

$\Theta < 1.05°$

As shown in Figure 5A, the average heights start at approximately the same value and increase with w_1, but as in the previous regime those of the bottom band increase much faster than those of the top band. The average heights for this regime are less than those of the previous regime. The plot for the area under the bands in Figure 5B demonstrates that this regime yields wholly smaller integrals compared to the previous one. The area under the bottom band once again increases at a higher rate than that of the top band. Note here that compared to the previous regime, the numerical difference between the heights and integrals of the top and bottom bands is much smaller, as the actual size of the bands themselves is much smaller.

Figure 5C shows select band structures in this regime. As all the bands are flatter than the control, it is visually apparent that none of these plots exit the flat-band scheme. Moreover, while in the $\Theta > 1.05°$ models band asymmetry was clearly visible, here we report only minor differences in band shape and height; symmetry is more or less maintained. The high peak about the Γ point that is present for $\Theta > 1.05°$ does not develop. Thus, while the height and size of the bottom band can analytically be shown to increase at a higher rate than that of the top band, as mentioned prior, this discrepancy can be concluded to be negligible and thus irrelevant.
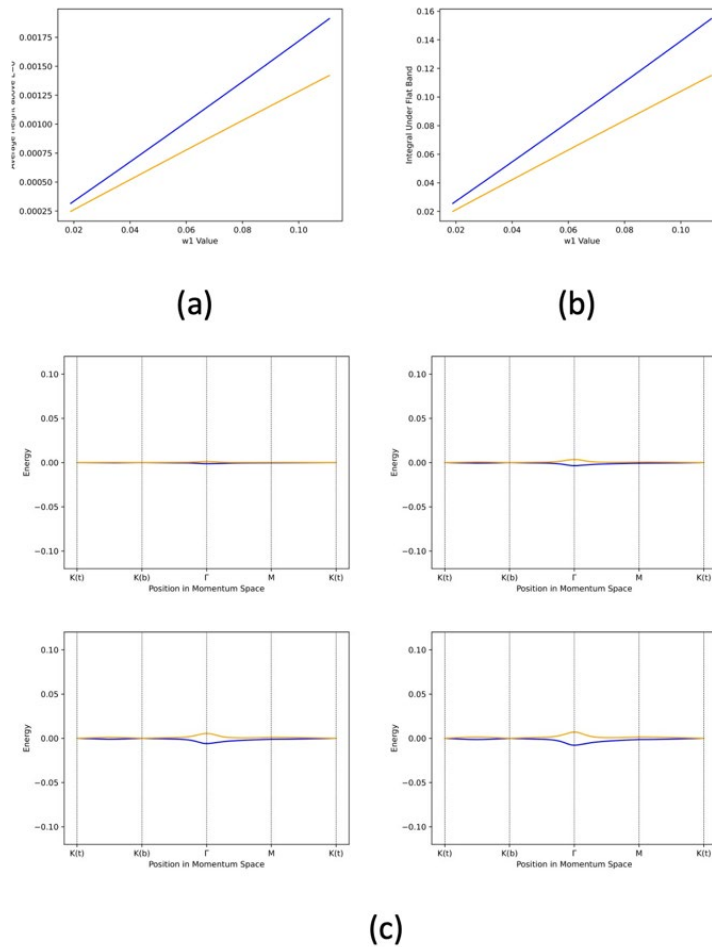
(a) (b)

(c)

Figure 5. Band height for $\Theta < 1.05°$. (*a*) Average height (energy) of all points making up band. (*b*) Integral under each band (for bottom band, this is instead additive inverse of integral, such that all integrals are positive). (*c*) Selected band structures — (*top left*): $w_1 = 0.0189eV$, or $\Theta \approx 0.18°$; (*top right*): $w_1 = 0.0519eV$, or $\Theta \approx 0.50°$; (*bottom left*): $w_1 = 0.0849eV$, or $\Theta \approx 0.81°$; (*bottom right*): control model.

Both Figures 6A and 6B support the conclusion that as we approach $w_1 = 0.0189$ eV or $\Theta \approx 0.18°$, the flatness of the bands is optimized. While the first indicates that the standard deviation of height is higher for the bottom band, the second suggests that the average magnitude of the gradient remains relatively the same for both bands. Taken altogether, band flatness increases as w_1 decreases, and the discrepancy between the flatness of the bands, and as with size and height, is negligible.
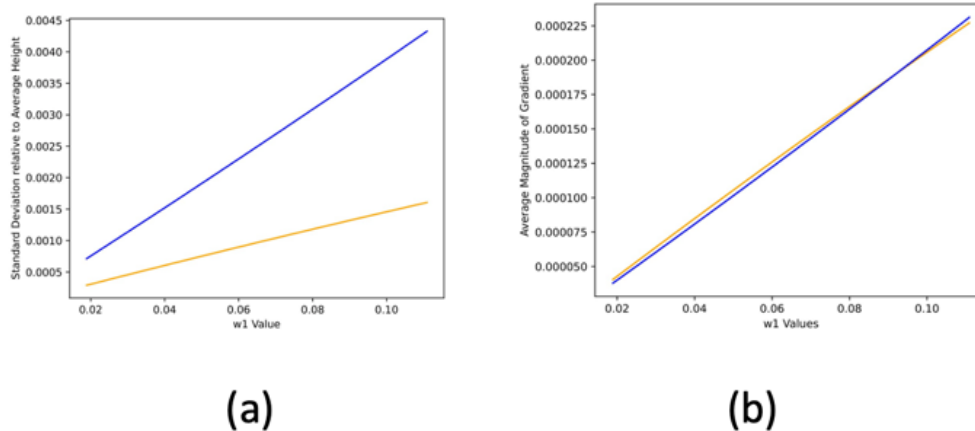
Figure 6. Band flatness for $\Theta < 1.05°$. (*a*) Standard deviation of heights of all points making up band. (*b*) Average magnitude of gradient (average of absolute values of gradient at each *k*-space point).

Discussion

Comparing the $\Theta > 1.05°$ and $\Theta < 1.05°$ regimes, we find both continuities and discrepancies between the two.

With regard to the former, the flat-band regime in the bottom band is only maintained up to a certain point, when the criteria of "low height" and "high flatness" in the bottom band are lost, and is not consistent up to $w_1 = 1.05$ eV. The top band remains in the regime even as we reach the $w_1 = 1.05$ eV limit. Taken together, upon reaching a certain value of w_1, and thus Θ, the flat-band regime will be destroyed, making it highly unlikely that superconductivity or other extraordinary properties will be present in the structure. Furthermore, as overall band flatness decreases with increases in w_1, the optimal magic-angle model, $\Theta \approx 1.05°$, has flatter bands than any and all models in the $\Theta > 1.05°$ regime. Therefore, it is also exceedingly unlikely that the magnitude or degree of extraordinary effects (superconductivity, etc.) will be higher for $\Theta > 1.05°$ than those obtained using conventional parameters. Thus, from an experimental standpoint, fabrication and study of $\Theta > 1.05°$ proportional angle-amplitude systems is unlikely to be fruitful with regard to yielding important or astounding scientific phenomena.

However, it is nonetheless true that the proportional angle-amplitude systems yield far, far flatter bands than standard-amplitude systems with the same twist angle (besides $\Theta \approx 1.05°$, as this is where the two types of systems intersect). By this, it is meant that if we fix the twist angle for two models to be some Θ, then the model where the amplitude values are adjusted to be proportional to the twist-angle, as demonstrated in this paper, would possess flatter bands than the traditional model where the amplitude values remain fixed and are not adjusted when Θ is changed. This is demonstrated in Figure 7; compared to its standard counterpart (the peaked, perfectly symmetric bands), the proportional angle-amplitude model (flat, slightly asymmetric bands) for the same $\Theta \approx 10°$ yields bands exponentially smaller and flatter in shape. Thus, this model essentially optimizes flatness of the bands for all angles by choosing optimal amplitude values. However, the standard optimal magic-angle model, $\Theta \approx 1.05°$, nonetheless possesses a flat-band regime that no proportional angle-amplitude systems for $\Theta > 1.05°$ can match or surpass.
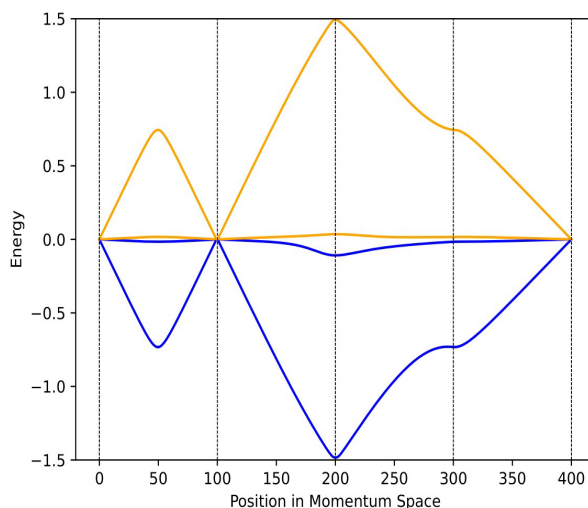
Figure 7. Band structures of proportional angle-amplitude model ($w_1 = 1.05$ eV) and standard-amplitude model ($w_1 = 0.11$ eV) for $\Theta \approx 10°$.

With regard to the $\Theta < 1.05°$ regime, we have that the flat-band regime is maintained in both bands. The overall flatness of the bands is greater for $\Theta < 1.05°$ than it is for $\Theta > 1.05°$ or the control model, and decreasing twist angle (and simultaneously w_1) yields flatter and flatter bands. Top-bottom band symmetry is furthermore maintained. Owing to these reasons, we have that the $\Theta < 1.05°$ regime, unlike its counterpart, represents the continuation of the flat-band regime in a form that presents itself as more extraordinary than the standard model, yielding flatter bands while not developing glaring abnormalities in the band structure (peaks, asymmetry between top and bottom bands, etc.) that would point to a loss of this remarkable flat-band regime.

Colloquially speaking, "the flatter the bands, the more interesting the structure". Extremely flat bands are not only an indication of remarkable properties, but it is no coincidence that the control model, which yields flatter bands than all other angles (for standard, fixed amplitude values), has the greatest amount and degree of said properties. The fact that the bands of the $\Theta < 1.05°$ regime are flatter than those of the optimal $\Theta \approx 1.05°$ model may result in it possessing more extensive properties, or even exhibiting new properties hitherto undiscovered. Given this, physical synthesis and further study of the models in this regime have the potential to provide an avenue for extraordinary discoveries.

Here, it is crucial to recall that there exists a limit to how low we can reduce the amplitudes, and by extension the twist angle. Lowering the interlayer amplitudes to smaller and smaller values would naturally decrease interlayer coupling, up until the point where coupling is too weak for the layers to form a coupled quantum system or for tunneling to persist. Thus, very small decreases in w_1, from 0.110 eV, may be the most promising avenue for study. In addition, proposed methods of decreasing w_1, the most promising of which is the use of an intercalation hBN spacer layer between the two layers, have not been tested in a laboratory setting or proven to conclusively function. The effect such a mechanism would have on the nature and dynamics of the system itself are also unknown, though they could potentially be substantial. Nevertheless, despite such concerns, we conclude that decreasing the Θ, w_1, and w_0 values proportionally, as demonstrated in this paper, have the potential to yield flatter bands and potentially more outstanding quantum, chemical, and electrical properties.

Our model concludes that by maintaining certain proportions between the parameters in the model, more extraordinary band structures can be produced. While we utilize simple linear ratios, more complex (linear with additional constants, quadratic, exponential, etc.) parameter relationships may yield even flatter bands and

even more extraordinary and astonishing properties. Simulation of models with such relationships and further experimentation would be required to determine whether results would be fruitful.

Acknowledgments

References

[1]   E. Y. Andrei and A. H. MacDonald, "Graphene bilayers with a twist," *Nature Materials*, vol. 19, no. 12, pp. 1265–1275, Nov. 2020. doi: 10.1038/s41563-020-00840-0. [Online]. Available: https://doi.org/10.1038%2Fs41563-020-00840-0.

[2]   G. Yang, L. Li, W. B. Lee, and M. C. Ng, "Structure of graphene and its disorders: A review," *Science and Technology of Advanced Materials*, vol. 19, no. 1, pp. 613–648, 2018, PMID: 30181789. doi: 10.1080/14686996.2018.1494493. eprint: https://doi.org/10.1080/14686996.2018.1494493. [Online]. Available: https://doi.org/10.1080/14686996.2018.1494493.

[3]   A. H. C. Neto, F. Guinea, N. M. R. Peres, K. S. Novoselov, and A. K. Geim, "The electronic properties of graphene," *Reviews of Modern Physics*, vol. 81, no. 1, pp. 109–162, Jan. 2009. doi: 10.1103/revmodphys.81.109. [Online]. Available: https://doi.org/10.1103% 2Frevmodphys.81.109.

[4]   A. Rozhkov, G. Giavaras, Y. P. Bliokh, V. Freilikher, and F. Nori, "Electronic properties of mesoscopic graphene structures: Charge confinement and control of spin and charge transport," *Physics Reports*, vol. 503, no. 2-3, pp. 77–114, Jun. 2011. doi: 10.1016/j.physrep. 2011.02.002. [Online]. Available: https://doi.org/10.1016%2Fj.physrep.2011.02.002.

[5]   Z. Sun and Y. H. Hu, "How magical is magic-angle graphene?" *Matter*, vol. 2, no. 5, pp. 1106–1114, 2020, issn: 2590-2385. doi: https://doi.org/10.1016/j.matt.2020.03.010. [Online]. Available: https://www.sciencedirect.com/science/article/pii/S2590238520301235.

[6]   A. Nimbalkar and H. Kim, "Opportunities and challenges in twisted bilayer graphene: A review," *Nano-Micro Letters*, vol. 12, no. 1, p. 126, Jun. 2020, issn: 2150-5551. doi: 10.1007/s40820-020-00464-8. [Online]. Available: https://doi.org/10.1007/s40820-02000464-8.

[7]   D. R. Cooper, B. D'Anjou, N. Ghattamaneni, *et al.*, "Experimental review of graphene," *ISRN Condensed Matter Physics*, vol. 2012, p. 501686, Apr. 2012, issn: 2356-7872. doi: 10.5402/2012/501686. [Online]. Available: https://doi.org/10.5402/2012/501686.

[8]   R. Bistritzer and A. H. MacDonald, "Moiré bands in twisted double-layer graphene," *Proceedings of the National Academy of Sciences*, vol. 108, no. 30, pp. 12233–12237, Jul. 2011. doi: 10.1073/pnas.1108174108. [Online]. Available: https://doi.org/10.1073%2Fpnas. 1108174108.

[9]   M. Yankowitz, S. Chen, H. Polshyn, *et al.*, "Tuning superconductivity in twisted bilayer graphene," *Science*, vol. 363, no. 6431, pp. 1059–1064, Mar. 2019. doi: 10.1126/science. aav1910. [Online]. Available: https://doi.org/10.1126%2Fscience.aav1910.

[10]   Y. Cao, V. Fatemi, A. Demir, *et al.*, "Correlated insulator behaviour at half-filling in magicangle graphene superlattices," *Nature*, vol. 556, no. 7699, pp. 80–84, Mar. 2018. doi: 10. 1038/nature26154. [Online]. Available: https://doi.org/10.1038%2Fnature26154.

[11]   A. L. Sharpe, E. J. Fox, A. W. Barnard, *et al.*, "Emergent ferromagnetism near three-quarters filling in twisted bilayer graphene," *Science*, vol. 365, no. 6453, pp. 605–608, Aug. 2019. doi: 10.1126/science.aaw3780. [Online]. Available: https://doi.org/10.1126%2Fscience. aaw3780.

[12]   Y. Saito, J. Ge, K. Watanabe, T. Taniguchi, and A. F. Young, "Independent superconductors and correlated insulators in twisted bilayer graphene," *Nature Physics*, vol. 16, no. 9, pp. 926– 930, Jun. 2020. doi: 10.1038/s41567-020-0928-3. [Online]. Available: https://doi.org/ 10.1038%2Fs41567-020-0928-3.

[13]   Y. Cao, V. Fatemi, S. Fang, *et al.*, "Unconventional superconductivity in magic-angle graphene superlattices," *Nature*, vol. 556, no. 7699, pp. 43–50, Mar. 2018. doi: 10.1038/nature26160. [Online]. Available: https://doi.org/10.1038%2Fnature26160.

[14]   B. L. Chittari, N. Leconte, S. Javvaji, and J. Jung, "Pressure induced compression of flatbands in twisted bilayer graphene," *Electronic Structure*, vol. 1, no. 1, p. 015001, Nov. 2018. doi: 10.1088/2516-1075/aaead3. [Online]. Available: https://doi.org/10.1088%2F25161075%2Faaead3.

[15]   H. Tang, F. Du, S. Carr, C. DeVault, O. Mello, and E. Mazur, "Modeling the optical properties of twisted bilayer photonic crystals," 2021. doi: 10.48550/ARXIV.2103.13600. [Online]. Available: https://arxiv.org/abs/2103.13600.

[16]   A. J. Wirth-Lima, M. G. Silva, and A. S. B. Sombra, "Comparisons of electrical and optical properties between graphene and silicene — a review," *Chinese Physics B*, vol. 27, no. 2, p. 023201, Feb. 2018. doi: 10.1088/1674-1056/27/2/023201. [Online]. Available: https://doi.org/10.1088/1674-1056/27/2/023201.

[17]   M. Vogl, M. Rodriguez-Vega, and G. A. Fiete, "Floquet engineering of interlayer couplings: Tuning the magic angle of twisted bilayer graphene at the exit of a waveguide," *Physical Review B*, vol. 101, no. 24, Jun. 2020. doi: 10.1103/physrevb.101.241408. [Online]. Available: https://doi.org/10.1103%2Fphysrevb.101.241408.

[18]   S. Carr, S. Fang, Z. Zhu, and E. Kaxiras, "Exact continuum model for low-energy electronic states of twisted bilayer graphene," *Physical Review Research*, vol. 1, no. 1, Aug. 2019. doi: 10.1103/physrevresearch.1.013001. [Online]. Available: https://doi.org/10.1103%2Fphysrevresearch.1.013001.

[19]   N. N. T. Nam and M. Koshino, "Lattice relaxation and energy band modulation in twisted bilayer graphene," *Physical Review B*, vol. 96, no. 7, Aug. 2017. doi: 10.1103/physrevb.96. 075311. [Online]. Available: https://doi.org/10.1103%2Fphysrevb.96.075311.

[20]   J. H. Wilson, Y. Fu, S. Das Sarma, and J. H. Pixley, "Disorder in twisted bilayer graphene," *Phys. Rev. Research*, vol. 2, p. 023325, 2 Jun. 2020. doi: 10.1103/PhysRevResearch.2. 023325. [Online]. Available: https://link.aps.org/doi/10.1103/PhysRevResearch.2. 023325.